HHS Public Access

Author manuscript

Nat Commun. Author manuscript; available in PMC 2016 January 02.

Published in final edited form as:

Nat Commun. ; 6: 8781. doi:10.1038/ncomms9781.

Asymmetric ring structure of Vps4 required for ESCRT-III disassembly

Christophe Caillat[1,2,†,7], **Pauline Macheboeuf**[1,2,†,7], **Yuanfei Wu**[3], **Andrew A McCarthy**[1,4], **Elisabetta Boeri-Erba**[4,5,6], **Gregory Effantin**[1,2,7], **Heinrich G. Göttlinger**[3], **Winfried Weissenhorn**[1,2,*,7], and **Patricia Renesto**[1,2]

[1]Univ. Grenoble Alpes, Unit of Virus-Host Cell interactions (UVHCI), F-38042 Grenoble, France

[2]CNRS, UVHCI, 71 avenue des Martyrs, F-38042 Grenoble, France

[3]Program in Gene Function and Expression, Program in Molecular Medicine, University of Massachusetts Medical School, Worcester, Massachusetts 01605, USA

[4]European Molecular Biology Laboratory (EMBL), Grenoble Outstation, 71 avenue des Martyrs, F-38042 Grenoble, France.

[4]Univ. Grenoble Alpes, Institut de Biologie Structurale (IBS), 71 avenue des Martyrs F-38044 Grenoble, France

[5]CNRS, IBS, 71 avenue des Martyrs F-38044 Grenoble, France

[6]CEA, IBS, 71 avenue des Martyrs F-38044 Grenoble, France

Abstract

The Vacuolar protein sorting 4 AAA-ATPase (Vps4) recycles endosomal sorting complexes required for transport (ESCRT-III) polymers from cellular membranes. Here, we present a 3.6 Å X-ray structure of ring-shaped Vps4 from *Metallosphera sedula* (MsVps4), seen as an asymmetric pseudohexamer. Conserved key interface residues are shown to be important for MsVps4 assembly, ATPase activity *in vitro*, ESCRT-III disassembly *in vitro* and HIV-1 budding. ADP binding leads to conformational changes within the protomer, which might propagate within the ring structure. All ATP binding sites are accessible and the pseudohexamer binds six ATP with micromolar affinity *in vitro*. In contrast, ADP occupies one high affinity and five low affinity binding sites *in vitro*, consistent with conformational asymmetry induced upon ATP hydrolysis.

[*]Corresponding and co-senior author: Winfried Weissenhorn, winfried.weissenhorn@ibs.fr.

[†]These authors contributed equally to this work.

Current address: [7]CEA-CNRS-Univ. Grenoble Alpes, Institut de Biologie Structurale (IBS), 71 avenue des Martyrs F-38044 Grenoble, France

Accession codes. Co-ordinates and structure factures have been deposited in the Protein Data Bank with accession IDs 4D80, 4D81, 4D82.

Author Contribution

P.R., H.G. and W.W. designed the experiments; P.R. carried out cloning; C.C. and P.R. performed protein purification and protein crystallization; X-ray diffraction data were collected by P.M., C.C. and W.W. Structure determination was performed by P.M., A. McC. and C.C.; C.C. and P.R. performed the ITC and ATPase assays. E.D. performed mass spectrometry analysis and G.E. protein quality control by electron microscopy. Y.W. performed the HIV-1 budding assay and C.C the ESCRT-III disassembly assay. W.W. wrote the manuscript with help from P.R.

Competing financial interests. The authors declare no competing financial interests.

The structure represents a snapshot of an assembled Vps4 conformation and provides insight into the molecular motions the ring-structure undergoes in a concerted action to couple ATP hydrolysis to ESCRT-III substrate disassembly.

Introduction

The ESCRT (*E*ndosomal *S*orting *C*omplex *R*equired for *T*ransport) machinery composed of ESCRT-0, -I, -II, -III and the Vps4 (*V*acuolar *p*rotein *s*orting 4) complex was originally discovered to catalyze plasma membrane receptor down regulation via multivesicular body formation[1,2]. Part of the ESCRT machinery including ESCRT-III and Vps4 are also recruited during cytokinesis[3,4] and budding of some enveloped viruses to catalyze membrane fission[5–7]. ESCRT-III is thought to assemble into helical filaments within membrane necks of budding vesicles or viruses or the cytokinetic midbody in order to constrict it and set the stage for membrane fission[8–10]. Vps4, a member of the type-I or meiotic clade of AAA family of proteins (*A*TPase *a*ssociated with various *a*ctivities)[11] disassembles ESCRT-III polymers from membranes[12] which might be coupled to the membrane fission reaction itself[13].

Proteins homologous to Vps4 and ESCRT-III are also present in the *Crenarchaeota* phylum of archaea where they catalyze final steps in cell division[1415], virus budding[16] and vesicle release[17].

Vps4 contains an N-terminal MIT (*M*icrotubule *I*nteracting and *T*rafficking) domain that interacts with C-terminal peptide motifs termed MIM (*M*IT domain *i*nteracting *m*otif) in activated eukaryotic and archaeal ESCRT-III proteins[4]. A linker region that varies in length between archaeal, yeast and mammalian Vps4 regulates its assembly and activity[18] and connects to the large ATPase domain, followed by the small ATPase domain and a C-terminal helix that packs against the large subdomain[19–21], thereby adopting a structure closely related to p97[22] and spastin[23]. Nucleotide binds into a cleft between the large and the small ATPase domains and induces conformational changes[24,25] associated with the ATPase reaction cycle[26]. Eukaryotic VPS4 has a β-domain inserted into the small ATPase domain[19,20,24] that recruits the VPS4 activator Vta1p/LIP5 implicated in assembly and ATPase activity[21,27–30]. Crenarchaeal Vps4 lacks the β-domain[29] and the regulatory factors are absent in *Crenarcheota*[31]. While human cells have two paralogs of *vps4* (VPS4A and VPS4B)[32], a single gene encoding Vps4 is present in archaea and yeast[2].

Vps4 oligomerizes upon nucleotide binding[12] like other AAA-type ATPases[33]. Exceptions are crenarchaeal Vps4, which can form dodecamers in the absence of nucleotides at non physiological protein concentrations[29,34]. Three cryo-electron microscopy structures of yeast Vps4 revealed two stacked ring structures with 12 or 14 subunits with substantial differences that might be attributed to different conformational states[35–37]. However, these structures were obtained with a catalytic inactive mutant (Glu233Gln) or in the presence of non-hydrolyzable ATP analogues. Recent work on archaeal and yeast Vps4 showed that wild-type proteins form hexamers in the presence of ATP, suggesting that the physiological oligomer is hexameric[29]. To date however only models of hexameric Vps4 exist that are

based on the p97 hexamer structure[22] and crystal packing contacts derived from 6-fold screw axis crystal packing interactions[19,20,24,25].

Here, we characterized the oligomeric state of the Vps4 homologue from *Metallosphera sedula* (MsVps4) that belongs to the phylum *Crenarchaeota*. While MsVps4 forms dodecamers at non-physiological protein concentrations in the absence of nucleotides, a MIT domain deletion mutant (MsVps4ΔMIT) assembles only into hexamers in solution. The catalytic activity of full length MsVps4 is around 10 times higher than that of MsVps4ΔMIT at physiological concentrations, consistent with a role for the MIT domain in ring assembly. The crystal structure of MsVps4ΔMIT revealed an asymmetric hexameric ring structure present in the asymmetric crystal unit. Further conformational changes occur upon nucleotide binding as revealed by the structure in complex with ADP and Mg^{2+}. The physiological relevance of two variable protomer interfaces was confirmed by site-directed mutagenesis *in vitro* and *in vivo* by probing oligomerization, ATPase activity, ESCRT-III disassembly and HIV-1 budding. We suggest that the structure may present a Vps4 intermediate state that is consistent with the conformational flexibility and asymmetry important for ATP-driven ESCRT-III disassembly.

Results

Oligomeric state of MsVps4 ΔMIT and enzymatic activity

Full length MsVps4 as well as Vps4 from *Sulfolobus solfataricus* (SsoVps4) and *Acidianus hospitalis* (AhosVps4) form concentration dependent dodecamers in the absence of nucleotides[29,34] but their oligomeric state is reduced to hexamers in the presence of ATP or ADP[29]. In order to determine the role of the N-terminal MIT domain in oligomerization, we purified a MIT domain deletion mutant that retained the linker region connecting the MIT domain to the ATPase domain (Figure 1a and Supplementary Fig. 1). As for full length protein, MsVps4ΔMIT (residues 75 to 369) oligomerizes in a concentration-dependent manner (Supplementary Fig. 2) without a 75°C heating step applied during SsoVps4 and AhosVps4 purification[29]. The largest oligomers elute at 14.1 ± 0.1 ml from a Superose 6 size exclusion chromatography (SEC) column, at a position slightly bigger than the marker protein catalase (Fig. 1b). Chemical cross linking of MsVps4ΔMIT in the absence and the presence of AMP-PNP and Mg^{2+} revealed a band migrating at ~ 200 kDa indicating hexamer formation (Fig. 1b, right panel). This was confirmed by native mass spectrometry that produced a molecular weight (MW) of 201.56 ± 0.01 kDa (calculated MW 201.36 kDa) and a slightly larger MW (211.77 ± 0.01 kDa) in the presence of AMP-PNP and Mg^{2+}(Fig. 1c). Although MsVps4ΔMIT hexamer formation can be observed at concentrations higher than 5–10 μM (Supplementary Fig. 2), no dodecamers are detected at concentrations up to 0.5 mM (20 mg/ml), corroborating the importance of the MIT domain for dodecamer assembly *in vitro*.

Comparison of the ATPase activity of full length MsVps4 versus MsVps4ΔMIT demonstrated that MsVps4ΔMIT is enzymatically active at 60 °C but requires a 40 times higher protein concentration. While full length MsVps4 was fully active at 0.25 μM with a turnover rate of ~16 ATP per minute, MsVps4ΔMIT attained similar activity at 10 μM (Fig. 1d). From these data we conclude that the presence of the MIT domain most likely favors

ATP dependent oligomer formation and/or stabilization, but is not essential for ATPase activity.

Crystal structure of Vps4ΔMIT

The structure of MsVps4ΔMIT was solved by molecular replacement and SAD techniques and the model was refined to a resolution of 3.6 Å (Table 1; Supplementary Fig. 3a). The asymmetric unit of the $P2_12_12_1$ space group contained one hexameric ring structure composed of the typical large ATPase domain and the small ATPase domain with its C-terminal helix packed against the large domain of the neighboring protomer (Fig. 2a). The β-domain inserted into a loop of the small ATPase domain in eukaryotic Vps4 (Figure 1a) is missing as in the related archaeal SsoVps4 homologue[29]. The 13 amino acid linker sequence plus 6 amino terminal residues that form a short β-strand (β') in mammalian VPS4A and B are disordered in all protomers. The orientation of the large ATPase domain with respect to the small one is the same in all six protomers and their Cα atoms superimpose with a r.m.s.d. of 0.62 Å. The ring structure has two-fold symmetry where opposing protomers make similar interactions (Fig. 2a). Three different protomer-protomer interfaces were identified between molecules A–B, B–C and C–D (interface D–E is the same as A–B, E–F corresponds to B–C and F–A to C–D), which are generated by a 10 and 15° rotation of the large ATPase domains in the different dimers (Fig. 2b). Each protomer-protomer interface can be split in two interacting surfaces, the conserved hydrophobic (H) interface between the small ATPase domain and the large ATPase domain from the neighboring protomer (Fig. 2c) and the variable (V) interface between two large ATPase domains from neighboring protomers (Fig. 2d). The H interface is hydrophobic and most of the interactions are conserved in all six interfaces (Supplementary Table 1). The V interface is dominated by polar interactions which vary substantially between the three different interprotomer interfaces (Supplementary Table 1). However, key interacting residues within the V and H interfaces are conserved between archaeal and human Vps4 (Supplementary Fig. 1). Superpositioning of the hexamer on itself by stepwise 60° rotations reveals the extensive conformational space that the pseudohexamer can adopt via its V and H interface in the absence of nucleotide (Supplementary Movie 1).

In order to probe the conformation upon nucleotide binding, hexameric MsVps4ΔMIT and a shorter MsVps4 construct lacking the linker region (MsVps4ΔL-MIT, residues 88–369) were crystallized in the presence of ADP and Mg^{2+}. Both constructs crystallized with $P6_5$ helical symmetry (Table 1) with similar H interfaces as observed in the hexamer structure and a V interface close the to A–B interface. ADP is coordinated between the large and small ATPase domains (Fig. 3a; Supplementary Fig. 3b and c) and P-loop residues Gly141, Cys142, Gly143, Lys144 and Thr145 (located on the large ATPase domain) bind the α- and β-phosphate groups of ADP while Tyr282, Arg310 and Val103 (located on the small ATPase domain) make hydrogen bonds with the sugar and the base. The base is stacked between the small and large ATPase domain in a pocket composed of residues Met146, Leu278 and Ala306 (Fig. 3a). Comparison of the nucleotide-free apo structure present in the ring structure showed that ADP binding induced a 23° rotation of the small ATPase domain compared to the large one (Fig. 3b and Supplementary Movie 2). Aligning the large ATPase domain of MsVps4ΔMIT with those of yeast Vps4 bound to ATPγS and ADP and mouse

SKD1/VPS4B in complex with ATP and ADP[19,24,25] showed significant differences in the position of the small ATPase domain including α6. ADP bound to MsVps4 occupies a similar position as ATPγS bound to yeast Vps4p while ADP bound to yeast Vps4p penetrates less into the binding pocket (Fig. 3c). Substantial differences are also observed between all known Vps4 apo structures (Fig.3d)[19,20,25,29,35], representing the overall conformational flexibility of the nucleotide-free structure.

The nucleotide binding cleft is open and accessible to nucleotides in all protomers of the apo structure. This is consistent with ITC experiments that demonstrated a 1:1 nucleotide binding ratio when ATP binding to MsVps4ΔMIT was determined at the MsVps4ΔMIT protein concentration that ensures nucleotide independent hexamer formation *in vitro*. The overall K_D of ATP interaction is 3.3 μM (Fig. 3e). Measurement of ADP binding to MsVps4ΔMIT showed that the MsVps4ΔMIT hexamer binds 5 ADP with low affinity (K_D 5.0 μM) and 1 ADP with higher affinity (K_D 0.4 μM) (Fig. 3f; 0.3 mM MsVps4ΔMIT). Together, these data indicate that MsVps4 can bind six ATP with low affinity and six ADP in a cooperative way *in vitro*.

Interface residues important for Vps4 assembly and ATPase activity

In order to validate the interactions present in the MsVps4ΔMIT hexamer we mutated residues conserved between archaeal and eukaryotic Vps4 homologues. Because removal of the His-tag from wild type MsVps4 was rather inefficient, the experiments with the mutants were carried out with N-terminally His-tagged MsVps4. The oligomeric state of interface mutants was first tested by SEC. This revealed four main peaks corresponding to dodecamers, hexamers, dimers and monomers for wild-type MsVps4 (Figure 4a). Notably, His-tagged MsVps4 has an approximately 6 times higher ATPase activity compared to untagged MsVps4, indicating that the presence of the tag seems to facilitate activation. First, we changed Phe126 and Met318 from the conserved H interface to alanine (Fig. 2c). SEC analyses of MsVps4 Phe126Ala showed a single peak corresponding to a monomer (Figure 4a), which was confirmed by SEC-MALLS (Supplementary Fig. 4). This indicates that the Phe side chain is crucial for oligomer formation and/or stability. Consistent with the defect in assembly, the Phe126Ala mutant has no ATPase activity (Table 2). In contrast, the Met318Ala mutation in close proximity to Phe126 (Fig. 2c) produces hexamers, dimers and monomers upon SEC analysis, but dodecamer formation is impaired (Figure 4a). Hexamer formation was confirmed by SAXS analysis (Supplementary Fig. 5). MsVps4 Met318Ala revealed an Rg of 4.64 nM and a calculated Dmax of 17.2 nM. Because the Rg and Dmax are smaller for the MsVps4ΔMIT structure (4.29 nm and 13.65 nm, respectively), we conclude that the MIT domain is flexibly linked and detached from the ring in this construct. Its ATPase activity is also enhanced by a factor of 1.5 compared to wild type MsVps4 (Table 2) corroborating the proposal that dodecamer formation is not required for ATPase activity[29].

Within the variable V interface the conserved Glu176 hydrogen bonds to Ser169 only in the C–D dimer, but not in the other dimer interfaces (A–B and D–E) (Fig. 2d, Supplementary Table 1). A double mutation of Glu176Ala and Glu174Ala within this variable V interface produced dodecamers, hexamers, dimers and monomers by SEC (Fig. 4a), however, its

ATPase activity was almost completely abolished (Table 2). Vice versa, a Ser169Ala mutant formed dodecamers and hexamers as analyzed by SEC (Fig. 4a), but still showed ATPase activity, suggesting that Glu174 is more important than Glu176 and its hydrogen bond to Ser169. Mutation of the two conserved Arg fingers, Arg259Ala and Arg260Ala, located within the V interface, abrogates dodecamer formation. However, the hexamers (and dimers and monomers) formed *in vitro* (Fig. 4a) have no ATPase activity (Table 2).

The N-terminal region comprising residues 88 to 95 is disordered in the ring structure, but form a short β'-strand and α-helix in the ADP-bound monomer structure, thus possibly acting as a flexible arm helping to reorient the MIT domain and its bound substrate during the ATP cycle. Mutation of Ile89 to Glu located in the β'-strand produced hexamers, but no dodecamers by SEC indicating a linker contribution in higher order assembly (Fig.4a). Although, the elution volume indicates a slightly larger hexameric structure, which is likely due to the displacement of the MIT domain thereby increasing the hydrodynamic radius of the complex. However, its ATPase activity was only slightly reduced (Table 2). Because substrate has been suggested to pass through the central pore of the ring structure, we mutated the pore loop 2 residue Glu214 to Tyr. SEC analysis revealed the same elution profile (dodedecamers, hexamers, dimers and monomers) as observed for wild-type MsVps4 (Fig. 4a), however, the ATPase activity was reduced to 8% of the wild type activity (Table 2). In summary, our mutagenesis data confirm the role of conserved key residues for MsVps4 assembly and demonstrate that ring formation is not sufficient for ATPase activity, which is coupled to pore loop 2 and V interface residues.

Because the above described key residues are conserved between archaeal and human VPS4 (A and B) (Supplementary Fig. 1, Supplementary Table 1), we mutated VPS4B homologous positions of three key residues that affect MsVps4 assembly and its ATPase activity. In order to test assembly of VPS4B *in vitro* in the presence of ATP, ATP hydrolysis must be inhibited. Therefore, the Phe160 (MsVps4 Phe126), Met350 (MsVps4 Met318) and Ile124 (MsVps4 Ile89) to alanine mutations were tested by SEC with a VPS4B Glu235Gln active site mutant. This showed that VPS4B Glu235Gln elutes as a monomer from a SEC column in the absence of ATP and as a hexamer in the presence of ATP (Fig. 4b). The Phe160 mutant is mostly monomeric, but still forms some higher order oligomers (Fig. 4b), which are absent in case of MsVps4. Met350, which is juxtaposed to Phe160 of the neighboring protomer in MsVps4 (Fig. 2c) and thus occupying the same hydrophobic pocket generated by hexamer assembly does no longer oligomerize (Figure 4b). Consistent with no significant oligomerization in the presence of ATP, both the Phe160 and Met350 mutant of wild type VPS4B have no ATPase activity (Table 2). Together, the data on the Phe160 and Met350 mutants indicate that these hydrophobic interactions are essential for VPS4B assembly and thus ATPase activity. The mutant Ile124Glu (MsVps4 Ile89) within the N-terminal β'-strand still assembled into hexamers, which elute slightly larger from a SEC column than the wild type (Fig.4b). However, in contrast to MsVps4 Ile89Glu, which still had ~ 85% ATPase activity, its ATPase activity is reduced to ~ 10% (Table 2).

Residues important for HIV-1 budding and ESCRT-III disassembly

To further confirm the physiological relevance of the two interfaces, we generated hVPS4A mutants and compared their effect on HIV-1 budding to the dominant negative effect of catalytic inactive VPS4A (GFP-hVPS4A-Glu228Gln) as described previously[38]. Over expression of the mutants that show no ATPase activity in the context of MsVps4 *in vitro*, Phe153Ala (MsVps4 Phe126), the double mutant Glu204Ala and Glu206Ala (MsVps4 Glu174 and 176) and the pore loop mutant Glu240Tyr (MsVps4 Glu214) in HIV-1 infected cells exerted a strong dominant negative effect on HIV-1 budding comparable to catalytic inactive hVPS4A-Glu228Gln. No or very small amounts of Gag are detected in the cell culture supernatant and Gag processing is affected as evident from the presence of CAp2 and CA cleavage products detected in cells (Fig. 5a and Supplementary Fig. 6). In contrast, the Val117Glu mutation had no effect on virus budding despite the detection of CAp2 in cells (Fig. 5a and Supplementary Fig. 6). Expression levels of GFP-hVPS4A wild type and mutants were comparable in these experiments (Fig. 5a and Supplementary Fig. 6). We conclude that the key residues identified in affecting ATPase activity *in vitro* are also important for hVPS4A function in HIV-1 budding. In addition, the mutation of Val117 to Glu that disrupted dodecamer but not hexamer assembly had little effect on its ATPase activity *in vitro* (Table 2, MsVps4Ile89Glu) and no influence on HIV-1 budding, further indicating that dodecamer assembly is not essential for its physiological function.

Because the dominant negative effect on HIV-1 budding observed with the above described mutants might be due to a defect in ESCRT-III disassembly, we tested a set of VPS4B mutants for their capacity to disassemble ESCRT-III CHMP2A-CHMP3 helical tubular structures *in vitro* as described before[39]. Fluorescein-labeled CHMP2A-CHMP3 tubes treated with wild type VPS4B and AMP-PNP (adenylyl-imidodiphosphate) and Mg^{2+} showed no changes in fluorescence emission intensity as a function of time (Fig. 5b). Dequenching, indicating disassembly of ESCRT-III CHMP2A-CHMP3, was measured as an increase in fluorescence emission when wild type VPS4B was added together with ATP and Mg^{2+} (Fig. 5b). As expected the catalytic mutant Glu235Gln did not disassemble the tubes, similar to the Ile124Glu and Phe160Ala mutants. The Met350Ala mutant had some disassembly activity and the Arg253Ala mutation within the V interface revealed an intermediate phenotype with ~50% disassembly activity over 20 minutes (Fig. 5b). We conclude that VPS4 catalyzed ESCRT-III disassembly requires conserved H and V interface residues.

Discussion

Here we report the crystal structure of the hexameric AAA-type ATPase Vps4 from *M. sedula*. Although several structures of Vps4 have been reported[19,20,24,25,29,35], none presented the native oligomeric conformation that is required for enzymatic activity[26]. The structure reveals an asymmetric pseudohexamer with three sets of opposing protomers making three different dimer-dimer interactions with neighboring protomers. The same principles of asymmetry have been described for nucleotide-free and nucleotide-bound bacterial AAA-type ClpX ring structures with nucleotide-loaded and free protomers facing each other (Supplementary Fig.7)[40,41]. Although the MsVps4 structure is nucleotide-free,

the conserved asymmetry indicates that opposing protomers may act together as reported for ClpX[40,41].

AAA-type ATPases bind nucleotide at the interface between the large and small ATPase domain of one protomer and the large ATPase domain from an adjacent protomer, generating six binding sites[26]. ADP binding to MsVps4 induces rotation of the small ATPase domain with respect to the large domain as reported for other Vps4 structures[19,24,25] and ClpX[40,41]. While this rotation is facilitated by a single coil linking the large and small ATPase domains of ClpX, the two MsVps4 domains are connected by the corresponding linker and the C-terminal helix 10, which might render the monomer more rigid. Notably, comparison of MsVps4 and ClpX demonstrates that nucleotide binding induces a much larger rotation of the small ATPase domain of ClpX than of MsVps4 (Supplementary Fig. 7). ClpX hexamers have been reported to bind four nucleotides in solution[42], although all six sites can also be occupied[41]. The crystal structure of MsVps4 shows that all nucleotide binding sites are accessible and ITC analyses demonstrate that MsVps4 can bind six ATP molecules with low affinity at room temperature with no apparent cooperativity, similar to the p97-VCP D1 ring that also binds six ATP per hexamer[43]. ADP bound in a cooperative way to MsVps4 with at least one high affinity and five low affinity binding sites, at a MsVps4ΔMIT protein concentration that allows hexamer formation independent of nucleotide *in vitro*. Nevertheless, we cannot exclude the possibility that some hexamer assembly may have contributed to the ITC signal. MsVps4 nucleotide binding *in vitro* differs from data on ClpX, which was reported to have two high affinity ATP binding sites and two low affinity sites at the nucleotide loading step[41]. Because the structures of ClpX adopt asymmetric conformations with 4-loaded and 2-unloaded states, it was suggested that the reaction cycle might pass via a 4-loaded 2-unloaded state or alternatively via a 5-loaded 1-unloaded state[40,41,44].

Vps4 ring assembly requires nucleotides[20,29], although archaeal Vps4 forms ring structures under non-physiological protein concentration and temperature conditions[29,34]. However, MsVps4 ring assembly is also induced by nucleotides under physiological conditions, because we measure significant ATPase activity at 0.25 μM concentration when MsVps4 is monomeric. Because MsVps4 rings bind six nucleotides *in vitro*, we propose that binding of six nucleotides leads to assembly of the ring structure and might thus present the starting or an early intermediate conformation at the onset of the nucleotide reaction cycle. In case of eukaryotic VPS4, assembly is further regulated by Ist1 and Vta1 upon ESCRT-III interaction, two factors that are absent in Crenarchaea[28,45].

Both full-length MsVps4 and MsVps4ΔMIT exert ATPase activity *in vitro*, which is substantial higher in the presence of the MIT domain, in contrast to data reporting increased ATPase activity in linker and MIT domain deletion mutants[46]. However, the linker region of eukaryotic Vps4 was also reported to be important for ring assembly and activity[18]. Our crystal structures reveal that the β'-strand at the N-terminus is ordered in the ADP-bound conformation and disordered in the nucleotide-free conformation, suggesting that this conformational flexibility might be important for MIT domain orientation. A mutation within the β'-strand abrogates MsVps4 dodecamer formation, but not hexamer formation and its ATPase activity is reduced. The corresponding VPS4B mutant also still forms

hexamers, but its ATPase activity is greatly reduced consistent with no ESCRT-III disassembly activity. The MIT domain is necessary to assemble MsVps4 dodecamers as its deletion produces only MsVps4 hexamers, which are enzymatically active consistent with the proposal that the physiological unit of Vps4 is hexameric[29]. This is further validated by two MsVps4 mutants (Met318Ala and Ile89Glu) that are hexameric and have wild-type like or slightly reduced ATPase activities. SAXS analysis of the MsVps4 Met318Ala mutant suggests hexameric ring structures with the MIT domains detached from the ring by the flexible linker. Because the MIT domain auto-inhibits ESCRT-III engagement[47] a conformation with the MIT domains assembled on top of the ring as observed by electron microscopy[35–37] might constitute an intermediate state during the activation cycle. The question remains whether there is a physiological role for dodecameric Vps4 such as recruiting multiple Vps4 hexamers to the site of ESCRT-III function thereby accelerating ESCRT-III disassembly? Notably double ring structures of ClpA unfold proteins faster than single ring ClpX structures[48].

The potential physiological relevance of the observed MsVps4 interfaces was confirmed by mutating V and H interface residues conserved between MsVps4, yeast Vps4 and human VPS4A and B. The effects of the mutations are twofold. They either influence VPS4 assembly leading to no or low ATPase activity or they have no affect on hexamer assembly, but are nevertheless physiologically inactive because the mutations disturb the ATPase cycle thereby inhibiting HIV-1 budding and ESCRT-III disassembly *in vitro*. The H interface mutant Phe126Ala (MsVps4) and its corresponding VPS4A and B mutants show defects in oligomerization, no ATPase activity, inhibit HIV-1 budding and ESCRT-III disassembly *in vitro*. The second H interface mutant Met318 (MsVps4), which form together with Phe126 a hydrophobic pocket is still hexameric and exerts ATPase activity, while its human VPS4B counterpart is defective in hexamer assembly and thus exerts no ATPase activity. It shows some residual ESCRT-III disassembly activity *in vitro*, which is consistent with the proposal that ESCRT-III polymers stimulate VPS4 assembly[28]. Reduced ATPase activity and hexamer formation *in vitro* were also reported for H interface mutants of SsoVps4 (Tyr121Asp and Phe328Ala)[29]. Notably, the effect of mutations within the V interface is similar in MsVps4 and human VPS4. A double mutation in the V interface (Glu174Ala, Glu176Ala) impaired the ATPase activity and blocked HIV-1 budding. Because the glutamate residues are ~ 22 Å distant from the active site glutamate 203, their substitution by alanine might inhibit the propagation of signals from one protomer to the next during the ATPase cycle. The arginine fingers (Arg259 and 260) have been implicated in nucleotide binding and ATP hydrolysis[49]. The structure shows that Arg259 makes different polar contacts depending on the dimer, while Arg260 has no clear stabilizing role in the unliganded MsVps4 structure. Nevertheless, the double mutation prevents dodecamer, but not hexamer formation. However, the hexamers lack ATPase activity in agreement with a previous report on SsoVps4[29]. Pore loop 1 and 2 mutants have been implicated in exerting a dominant negative effect on HIV-1 budding[20,25] and ESCRT-III disassembly[46]. Mutation of Glu214 (MsVps4) to Tyr had no effect on dodecamer and hexamer assembly, but reduced the ATPase activity to less than 10% and its corresponding mutation in VPS4A (Glu240Tyr) blocked HIV-1 budding almost completely, similar to the reported Glu240Ala mutation[25]. Recent work showed that this conserved glutamate residue affects substrate binding within

the pore[47]. This is also consistent with the importance of pore loop residues for ESCRT-III unfolding when passing through the central pore[50]. The defect induced by the alanine and tyrosine mutations indicates that the negative charge of the glutamate is critical for the ATPase cycle and thus for ESCRT-III unfolding.

In summary, we identified several key residues that are located at the conserved V and H interfaces, far from the active site, but important for MsVps4 and human VPS4 function. Based on these observations we propose the following mode of action for Vps4. First, Vps4 assembles in the presence of ATP molecules into a stable asymmetric ring structure that might resemble our nucleotide-free structure. ATP hydrolysis then leads to different intermediate states including potentially one when the ring has one high affinity binding site and five low affinity binding sites for ADP (Figure 6). The different potential conformations adopted by the three opposing dimers coupled to the movement of the small ATPase domain upon nucleotide binding and release indicates how these conformational motions might be propagated throughout the ring structure. Key interface residues such as Glu174 and Glu176 (located on α3), the arginine finger and the pore loop residue Glu214 are important for transferring the ATPase activity from two opposing protomers to their neighboring set. This may generate flexing motions of the whole ring as suggested for ClpX[40] whereby the nucleotide reaction cycle, free state, ATP binding, hydrolysis and ADP-bound states is converted into mechanical work[41]. The asymmetric structure of MsVps4 provides a snapshot of the conformational flexibility of a hexameric Vps4 AAA-type ATPase, which will help to understand its reaction cycle that is most likely similar to other asymmetric AAA-type ATPases functioning as proteases, helicases and unfoldases[51–53].

Methods

Cloning, expression and purification of MsVps4 and hVPS4B

The gene encoding the full length MsVps4 or truncated constructs were amplified by PCR from genomic DNA and using High-Fidelity PCR master mix (Phusion, Finnzymes) and gene-specific primers encoding a Tobacco Etch Virus (TEV) site. M*utations were introduced* by *overlapping PCR.* The resulting products were cloned into the pDEST-17 vector using the Gateway cloning system from Invitrogen and following the manufacturer's instructions. The gene encoding the full length human VPS4B (hVPS4B) was cloned into the pProExHT vector. Mutations were introduced by overlapping PCR.The sequences of all constructs were confirmed by DNA sequencing.

Purification of MsVps4 constructs

The *E. coli* C41(DE3) strain was used as the host for protein expression. The cells were grown in LB medium supplemented with ampicillin (100μg/ml) to an absorbance of approximately 0.5 and expression was induced for 1 hour at 37 °C by addition of 0.1 mM isopropyl-β-D-thiogalactopyranoside (IPTG). To obtain selenomethionine (Se-Met) incorporated MsVps4ΔMIT, cells were cultured in M9 medium supplemented with Se-Met (60 mg/l) and other natural amino acids. Induction conditions were the same as for the native protein. The cells were pelleted by centrifugation (5,000 × *g*, 20 min), resuspended in lysis buffer (50 mM Tris pH 8.8, 50 mM NaCl, 10 mM imidazole, 1% CHAPS and

Complete Protease Inhibitor® (*Roche* Diagnostics)), then disrupted by sonication. After centrifugation (20,000 rpm, 30 min, 4°C) the bacterial lysate was applied onto a Ni^{2+}-NTA column (Qiagen) for affinity purification. After extensive washings (50 mM Tris pH 8.8, 50 mM NaCl 50, 20 mM imidazole) the protein was eluted in presence of 300 mM imidazole. The fractions containing MsVps4ΔMIT were pooled and incubated overnight at room temperature with (Tobacco Etch Virus) TEV (0.2 mg /10 mg of protein) and dialyzed against 50 mM Tris pH 8.8, 50 mM NaCl. The TEV protease and uncleaved protein were removed by passing the solution through Ni^{2+}-NTA column (Qiagen) and collecting the unbound protein. Cleaved MsVps4ΔMIT was then concentrated to 150–200 μM using an Amicon 400 concentrator with 30-kDa cutoff membrane and purified by anion-exchange chromatography (monoQ) and Superose 6 size exclusion chromatography (SEC) on an ÄKTA FPLC™ system (GE Healthcare, UK). The peak fractions were analyzed on 12% SDS-PAGE and Commassie blue staining and concentrated to 10 mg/ml for crystallization. Incorporation of Se-met was confirmed by mass spectrometry. Extensive crystallization trials that included 576 conditions in 96-well sitting-drop vapor diffusion format were performed on various constructs at the high-throughput crystallization facility of the EMBL Grenoble outstation. Following optimization, crystals used for diffraction studies were grown at 20°C in hanging drop vapour diffusion plates. Wild type and mutant MsVps4 were purified by the same protocol.

Purification of hVPS4B constructs

The E. coli C41(DE3) strain was used as the host for protein expression. The cells were grown in LB medium supplemented with ampicillin (100μg/ml) to an absorbance of approximately 0.8 and expression was induced over night at 20 °C by addition of 0.1 mM IPTG. The cells were pelleted by centrifugation (5,000 × g, 20 min), resuspended in lysis buffer (50 mM Tris pH 8.0, 150 mM NaCl, 10 mM imidazole and Complete Protease Inhibitor® (Roche Diagnostics)), then disrupted by sonication. After centrifugation (20,000 rpm, 30 min, 4°C) the bacterial lysate was applied onto a Ni^{2+-}NTA column (Qiagen) for affinity purification. After extensive washing (50 mM Tris pH 8.0, 150 mM NaCl 50, 20 mM imidazole) the protein was eluted in presence of 300 mM imidazole. The fractions containing MsVps4ΔMIT were pooled and incubated overnight at room temperature with (Tobacco Etch Virus) TEV (0.2 mg /10 mg of protein) and dialyzed against 25 mM Hepes, 150 mM NaCl, 10 mM Imidazole. The TEV protease and uncleaved protein were removed by passing the solution through Ni^{2+}-NTA column (Qiagen) and collecting the unbound protein. Cleaved MsVps4ΔMIT was concentrated to 80–150 μM using an Amicon 400 concentrator with 10-kDa cutoff membrane and purified by Superose 6 size exclusion chromatography (SEC) on an ÄKTA FPLC™ system (GE Healthcare, UK) in a buffer containing 25 mM Hepes pH 7.5, 150 mM NaCl, 0.5 mM, DTT.

Chemical cross-linking

Untagged MsVps4ΔMIT was purified by SEC (Superose 6) in 50 mM Hepes pH 7.5 and the fractions corresponding to oligomers were cross-linked for 20 minutes at room temperature with 0.05% glutaraldehyde, as reported for the yeast Vps4p complexes. Following addition of an equal volume of 1M glycine pH7 to quench the reaction, the sample was re-injected on the superose 6 and peak fractions were collected for mass spectrometry.

Mass spectrometry

Cross-linked samples were desalted and buffer exchanged using ultrafiltration (Vivaspin 500, Sartorius) with a 50 kDa cutoff, then diluted to a concentration of 5–8 μM in 250 mM NH_4Ac at pH7. Protein complex ions were generated using a nanoflow electrospray (nano-ESI) source. Mass spectrometry analyses were carried out on a quadrupole time-of-flight mass spectrometer (Q-TOF Ultima, Waters Corporation, Manchester, U.K.). The instrument was modified for the detection of high masses. The following instrument parameters were used: capillary voltage up to 1.2–1.3 kV, cone potential = 40 V, RF lens-1 potential = 40 V, RF lens-2 potential = 1 V, aperture-1 potential = 0 V, collision energy = 20–40 V, and microchannel plate (MCP) = 1900 V. All mass spectra were calibrated externally using a solution of cesium iodide (6 mg/mL in 50% isopropanol) and were processed with the Masslynx 4.0 software (Waters Corporation, Manchester, U.K.).

ATPase activity

The ATPase activity of the different constructs was carried out at 60°C and *according* to the manufacturer's instructions using the QuantichromeTM ATPase/GTPase Assay Kit (BioAssay Systems). Solutions containing 0.1 μM – 10 μM MsVps4, 25 mM Hepes pH 7.5, 50 mM NaCl, 2 mM MgCl2 and 1mM ATP were prepared on ice. They were then incubated at 60°C for various times (1 to 30 min). For hVPS4B, solutions containing 10 μM hVPSB, 25 mM Hepes pH 7.5, 150 mM NaCl were prepared on ice, 10 mM MgCl2 and 1mM ATP were added at the start of the experiment. They were then incubated at 37°C for various times (10 to 30 min). The reaction was stopped on ice and reagent was added and incubated 30 min at room temperature. The complex formed by the reagent and free phosphate was detected by absorbance at 620 nm using a plate reader. A sodium phosphate standard curve was used to estimate the amount of phosphate released during ATP hydrolysis.

Isothermal titration calorimetry

The binding constants of ATP to MsVps4ΔMIT were measured by ITC (MicroCal Inc.). All samples used in the ITC experiments were dialyzed against 25mM Hepes pH 7.5, 50 mM NaCl and 2 mM $MgCl_2$. The ITC measurements were performed at 15°, 20° and 25°C by making 28 injections (10 μl) of ATP or ADP to 1.4 ml of MsVps4ΔMIT. The concentrations of the MsVps4ΔMIT and ATP were 100 μM or 300 μM and 1 mM, respectively. Curve fitting was performed with the MicroCal Origin software. The experiments were done in triplicate.

ESCRT-III CHMP2A-CHMP3 polymer disassembly

CHMP2AΔC/CHMP3 polymers were assembled as described previously[39]. For amine specific labelling of the co-polymer, NHS ester (or succinimidyl ester) of Alexa Fluor® 488 (Life Technologies) was dissolved in anhydrous DMSO and added to the co-polymer solution in HBS. The reaction was carried out at 4°C over night at a final concentration of 2 mg/ml of protein and 300 μM of the fluorophore. The reaction mixture was centrifuged and the pellet was extensively washed in order to remove free fluorophore and resuspended in HBS. The efficiency of the labelling was estimated by measuring the absorbance of the protein at 280 nm (taking in account the absorbance of the dye at 280 nm) and the

fluorescence of Alexa Fluor 488 at 495 nm and the estimated value was 1.5 dye per CHMP2AΔC/CHMP3 dimer. The disassembly of the polymer was monitored on a BMG FLUOstar OPTIMA Microplate Reader. The different constructs of hVPS4B (10 μM) were mixed with the CHMP2AΔC/CHMP3 polymers (3μM) in reaction volumes of 100 μl HBS. After about 150 seconds, ATP/Mg (1mM/10mM) was added to the mixtures containing hVPS4B wt, hVPS4B E235Q, hVPS4B I124E, hVPS4B M350A, hVPS4B F160A, and hVPS4B R253A. After about 150 seconds, AMPPNP/Mg (1mM/10mM) was added to the mixture containing hVPS4B wt. Emission intensity was measured at 520 nm as a function of time by exciting the Alexa 488 at 490 nm.

Mammalian expression plasmids and HIV-1 budding assay

The GFP-VPS4A mutations were generated via overlapping PCR and the correctness of the sequence was confirmed by DNA sequencing. To examine the effects of wild-type and mutated GFP-VPS4A on HIV-1 release, 293T (ATCC CRL-3216) cells (1.2×10^6) were seeded into T25 flasks and transfected 24 hr later using a calcium phosphate precipitation technique. The cultures were transfected with 1 μg Vpu-negative proviral DNA ($HIV\text{-}1_{HXB2}$) together with expression vectors for wild-type or mutated GFP-VPS4A. The total amount of transfected DNA was brought to 8 μg with carrier DNA (pTZ18U). Twenty-four hours post-transfection, the cells were lysed in radioimmunoprecipitation assay buffer (140 mM NaCl, 8 mM Na_2HPO_4, 2 mM NaH_2PO_4, 1% NP-40, 0.5% sodium deoxycholate, 0.05% SDS), and the culture supernatants were clarified by low-speed centrifugation and passed through 0.45 μm filters. Virions released into the medium were pelleted through 20% sucrose cushions by ultracentrifugation for 2 hr at 27,000 rpm and 4°C in a Beckman SW41 rotor. Pelletable material and the cell lysates were analyzed by SDS-PAGE and western blotting, using the anti-HIV CA antibody 183-H12-5C to detect Gag proteins. GFP-VPS4A was detected using an anti-GFP antibody (Molecular Probes/Life Technologies).

SAXS analysis of MsVps4

Small Angle X-ray Scattering Experiment (SAXS) Data Collection and Analysis. MsVPS4 M318A was purified as described above (his tag was cleaved) and used for the SAXS experiments. SAXS experiments were performed at the BM29 BioSAXS beamline at the ESRF (Grenoble, France). Data were collected using an online size-exclusion chromatography (SEC). 500 μl of MsVPS4 M318A at 220 μM was injected on a superose 6 10/300 GL, equilibrated in 50 mM Tris pH 8.8 50 mM NaCl. Data corresponding to the elution peek of MsVPS4 M318A was analysed; the data was normalized to the intensity of the incident beam, the scattering of the buffer was subtracted and the resulting intensities were scaled for concentration. Data processing and analysis were performed using the ATSAS package[54] and molecular weights were estimated[55]. The final merged scattering data were further evaluated using PRIMUS[56]. The isotropic scattering intensity I(q) was transformed to the distance distribution function P(r) using the program GNOM, which was also used to calculate the maximum dimensions of the particle, the Dmax[57].

Size exclusion chromatography and multi-angle laser light scattering

SEC was performed with a superose 6. The column was equilibrated in 50 mM Tris pH 8.8 50 mM NaCl and MsVps4 Phe126Ala was injected at 200 μM. The experiment was

performed with multi-angle laser light scattering (MALLS) using a DAWN-EOS detector (Wyatt Technology Corp., Santa Barbara, CA) and refractive index measurement using a RI2000 detector (Schambeck SFD). Light scattering intensities were measured at different angles relative to the incident beam, and analysis of the data was performed with the ASTRA software (Wyatt Technology Corp., Santa Barbara, CA).

Crystallization, data collection and structure determination

MsVps4ΔMIT was crystallized in 20 mM Tris, 50 mM NaCl, 0.2 M sodium malonate pH 7 and19% PEG 3350 by mixing 1 μl of the reservoir to 1 μl of protein at 10.8 mg/ml. The crystals were cryoprotected in the same conditions containing 25% ethylene glycol and flash cooled in liquid N_2 before data collection. Se-Met derivatized crystals of MsVps4ΔMIT grew under the same conditions. A data set from a Se-Met crystal was collected at 0.97 Å wavelength to 3.6 Å resolution on the ID14-EH4 beam line at the European Synchrotron Radiation Facility (ESRF, Grenoble, France). Data were processed with the program XDS[58] and the crystals belong to space group $P2_12_12_1$ (Table 1).

The structure was solved by molecular replacement using the program Phaser[59] and a Vps4 model generated with the Phenix Ensembler program[60] using human Vps4 (PDB code 1XWI), yeast Vps4 (PDB code 2RKO), yeast Vps4 (PDB code 2QP9) and yeast (PDB code 3EIH) as input models. The molecular replacement model was confirmed by the single anomalous dispersion method employing the data set collected at the peak wavelength (0.9791 Å). The phases were improved and initial model building was performed with the program Crank2[61] using both the anomalous signal and the molecular replacement solution described previously. Further model building was completed manually with Coot[62] and the model was refined with REFMAC[63] to an R_{factor} of 26.4% and R_{free} of 31.8%. The model contains chain A residues 97 to 369, chain B residues 98 to 367, chain C residues 96 to 367, chain D residues 97 to 369, chain E residues 96 to 367 and chain F residues 96 to369. The N-terminal residues 75 to 95 were disordered in all protomers and 82.92/8.35 % of the residues are within the most favored and allowed regions of a Ramachandran plot[64].

Crystallization and structure solution of MsVps4 in complex with ADP

Two constructs of MsVps4 were crystallized with ADP: MsVps4ΔMIT (residues 75 to 369) and MsVps4ΔL-MIT (residues 88 to 369). Final ADP/ MsVps4ΔL-MIT cocrystals were grown by mixing 1 μl of 8 mg/ml MsVps4ΔL-MIT, 5 mM ADP, 10 mM $MgCl_2$, and 1 μl of the reservoir solution containing 40% (w/v) polyethylene glycol 200 (PEG200) and 100 mM Tris-HCl buffer (pH 8.8). Crystals were directly flash cooled in liquid N_2 at 100 K. Data were collected on beamline BM14 at the ESRF at a wavelength of 0.9737 Å. Final ADP/ MsVps4ΔMIT cocrystals were grown by mixing 1 μl of 10 mg/ml MsVps4ΔMIT, 5 mM ADP, 5 mM $MgCl_2$, and 1 μl of the reservoir solution containing 1,4 M sodium/potassium phosphate pH 5.6 (1.26 M sodium dihydrogen phosphate monohydrate and 0.14 M di-potassium hydrogen phosphate) and 7.5% (v/v) glycerol. Crystals were soaked in the reservoir solution supplemented with 25 % (v/v) glycerol and flash cooled in liquid N_2 at 100 K. Data were collected on beam line ID23-2 at the ESRF.

Data were processed with the program XDS[58]. Both crystals belong to space group $P6_5$ but with different cell dimensions (Table 1). The structures were solved by molecular replacement using the program Phaser[59] and the apo MsVps4ΔMIT model. The model was rebuilt using COOT[62] and refined using REFMAC[63], Phenix[65] and PDB_REDO web server[66]. Statistics for data reduction and structure refinement are presented in Table 1. The models were evaluated by using COOT and Phenix. In both structures the nucleotides gave clear electronic density and were present in all MsVps4 subunits. For the ADP/ MsVps4ΔL-MIT complex, one molecule of ADP and one molecule of MsVps4ΔL-MIT containing residues 97 to 363 are present in the asymmetric unit. The structure was refined against 2.4 Å data to an R/R_{free} of 20.6/26.6% and 98.1 /99.6 % of the residues are within the most favored and allowed regions of a Ramachandran plot. For the ADP/ MsVps4ΔMIT complex, three molecules of ADP and three molecules of MsVps4ΔMIT are present in the asymmetric unit. MsVps4ΔL-MIT chain A contains residues 97 to 366, chain B contains residues 88 to 366 and chain C contains residues 90 to 366. The structure was refined against 3.2 Å data to an R/Rfree of 22.9/26.8% and 96.9/99.9 % of the residues are within the most favored and allowed regions of a Ramachandran plot.

Structure analysis

Molecular graphics figures were generated with PyMOL (W. Delano; http://www.pymol.org). Further details are described in the supplementary information.

Supplementary Material

Refer to Web version on PubMed Central for supplementary material.

Acknowledgments

This work was initiated by the ANR (ANR-08-BLAN-0271) and supported by the ANR (ANR-12-BSV8-0004), by the NIH/NIAID grant AI029873 (H.G) and the Institut Universitaire de France (W.W.). G.E. was supported by a post-doctoral fellowship from the ANRS. We acknowledge the platforms of the Grenoble Instruct center (ISBG; UMS 3518 CNRS-CEA-UJF-EMBL) supported by the French Infrastructure for Integrated Structural Biology Initiative FRISBI (ANR-10-INSB-05-02) and GRAL (ANR-10-LABX-49-01) within the Grenoble Partnership for Structural Biology (PSB). We further thank the ESRF-EMBL Joint Structural Biology Group for access and support at the ESRF beam lines, J. Marquez (EMBL) from the crystallization platform, M. Jamin (UVHCI) for SEC-MALLS analysis, L. Signor (IBS, Grenoble) and P. A. Klein (IBS, Grenoble) for mass spectrometry, N. Pannu (Leiden University) for help with Crank2 and J. Radzimanowski for help with SAXS data analysis. The following reagent was obtained through the AIDS Research and Reference Reagent Program, Division of AIDS, NIAID, NIH: HIV-1 p24 monoclonal antibody (183-H12-5C) from Dr. Bruce Chesebro and Kathy Wehrly.

References

1. Henne WM, Buchkovich NJ, Emr SD. The ESCRT pathway. Dev Cell. 2011; 21:77–91. [PubMed: 21763610]
2. Babst M, Davies BA, Katzmann DJ. Regulation of Vps4 during MVB sorting and cytokinesis. Traffic. 2011; 12:1298–1305. [PubMed: 21658171]
3. Agromayor M, Martin-Serrano J. Knowing when to cut and run: mechanisms that control cytokinetic abscission. Trends Cell Biol. 2013; 23:433–441. [PubMed: 23706391]
4. McCullough J, Colf LA, Sundquist WI. Membrane fission reactions of the mammalian ESCRT pathway. Annu Rev Biochem. 2013; 82:663–692. [PubMed: 23527693]
5. Votteler J, Sundquist WI. Virus budding and the ESCRT pathway. Cell Host Microbe. 2013; 14:232–241. [PubMed: 24034610]

6. Martin-Serrano J, Neil SJ. Host factors involved in retroviral budding and release. Nat Rev Microbiol. 2011; 9:519–531. [PubMed: 21677686]
7. Usami Y, et al. The ESCRT pathway and HIV-1 budding. Biochem Soc Trans. 2009; 37:181–184. [PubMed: 19143627]
8. Fabrikant G, et al. Computational model of membrane fission catalyzed by ESCRT-III. PLoS Comput Biol. 2009; 5:e1000575. [PubMed: 19936052]
9. Bajorek M, et al. Structural basis for ESCRT-III protein autoinhibition. Nat Struct Mol Biol. 2009; 16:754–762. [PubMed: 19525971]
10. Guizetti J, et al. Cortical Constriction During Abscission Involves Helices of ESCRT-III-Dependent Filaments. Science. 2011; 331(6024):1616–1620. [PubMed: 21310966]
11. Frickey T, Lupas AN. Phylogenetic analysis of AAA proteins. J Struct Biol. 2004; 146:2–10. [PubMed: 15037233]
12. Babst M, Wendland B, Estepa EJ, Emr SD. The Vps4p AAA ATPase regulates membrane association of a Vps protein complex required for normal endosome function. EMBO J. 1998; 17:2982–2993. [PubMed: 9606181]
13. Weissenhorn W, Poudevigne E, Effantin G, Bassereau P. How to get out: ssRNA enveloped viruses and membrane fission. Current Opinion in Virology. 2013; 3:159–167. [PubMed: 23583788]
14. Lindas AC, Karlsson EA, Lindgren MT, Ettema TJ, Bernander R. A unique cell division machinery in the Archaea. Proc Natl Acad Sci U S A. 2008; 105:18942–18946. [PubMed: 18987308]
15. Samson RY, Obita T, Freund SM, Williams RL, Bell SD. A role for the ESCRT system in cell division in archaea. Science. 2008; 322:1710–1713. [PubMed: 19008417]
16. Snyder JC, Samson RY, Brumfield SK, Bell SD, Young MJ. Functional interplay between a virus and the ESCRT machinery in archaea. Proc Natl Acad Sci U S A. 2013; 110:10783–10787. [PubMed: 23754419]
17. Ellen AF, et al. Proteomic analysis of secreted membrane vesicles of archaeal Sulfolobus species reveals the presence of endosome sorting complex components. Extremophiles. 2009; 13:67–79. [PubMed: 18972064]
18. Shestakova A, Curtiss M, Davies BA, Katzmann DJ, Babst M. The linker region plays a regulatory role in assembly and activity of the Vps4 AAA ATPase. J Biol Chem. 2013; 288:26810–26819. [PubMed: 23913684]
19. Inoue M, et al. Nucleotide-Dependent Conformational Changes and Assembly of the AAA ATPase SKD1/VPS4B. Traffic. 2008; 9:2180–2189. [PubMed: 18796009]
20. Scott A, et al. Structural and mechanistic studies of VPS4 proteins. EMBO J. 2005; 24:3658–3669. [PubMed: 16193069]
21. Azmi IF, et al. ESCRT-III family members stimulate Vps4 ATPase activity directly or via Vta1. Dev Cell. 2008; 14:50–61. [PubMed: 18194652]
22. Zhang X, et al. Structure of the AAA ATPase p97. Mol Cell. 2000; 6:1473–1484. [PubMed: 11163219]
23. Roll-Mecak A, Vale RD. Structural basis of microtubule severing by the hereditary spastic paraplegia protein spastin. Nature. 2008; 451:363–367. [PubMed: 18202664]
24. Xiao J, Xia H, Yoshino-Koh K, Zhou J, Xu Z. Structural characterization of the ATPase reaction cycle of endosomal AAA protein Vps4. J Mol Biol. 2007; 374:655–670. [PubMed: 17949747]
25. Gonciarz MD, et al. Biochemical and Structural Studies of Yeast Vps4 Oligomerization. J Mol Biol. 2008; 384:878–895. [PubMed: 18929572]
26. Hill CP, Babst M. Structure and function of the membrane deformation AAA ATPase Vps4. Biochim Biophys Acta. 2012; 1823:172–181. [PubMed: 21925211]
27. Lottridge JM, Flannery AR, Vincelli JL, Stevens TH. Vta1p and Vps46p regulate the membrane association and ATPase activity of Vps4p at the yeast multivesicular body. Proc Natl Acad Sci U S A. 2006; 103:6202–6207. [PubMed: 16601096]
28. Shestakova A, et al. Assembly of the AAA ATPase Vps4 on ESCRT-III. Mol Biol Cell. 2010; 21:1059–1071. [PubMed: 20110351]

29. Monroe N, et al. The oligomeric state of the active Vps4 AAA ATPase. J Mol Biol. 2014; 426:510–525. [PubMed: 24161953]
30. Vild CJ, Li Y, Guo EZ, Liu Y, Xu Z. A novel mechanism of regulating the ATPase VPS4 by its cofactor LIP5 and the endosomal sorting complex required for transport (ESCRT)-III protein CHMP5. J Biol Chem. 2015; 290:7291–7303. [PubMed: 25637630]
31. Hobel CF, Albers SV, Driessen AJ, Lupas AN. The Sulfolobus solfataricus AAA protein Sso0909, a homologue of the eukaryotic ESCRT Vps4 ATPase. Biochem Soc Trans. 2008; 36:94–98. [PubMed: 18208393]
32. Scheuring S, et al. Mammalian cells express two VPS4 proteins both of which are involved in intracellular protein trafficking. J Mol Biol. 2001; 312:469–480. [PubMed: 11563910]
33. Lupas AN, Martin J. AAA proteins. Curr Opin Struct Biol. 2002; 12:746–753. [PubMed: 12504679]
34. Moriscot C, et al. Crenarchaeal CdvA forms double-helical filaments containing DNA and interacts with ESCRT-III-like CdvB. PLoS One. 2011; 6:e21921. [PubMed: 21760923]
35. Hartmann C, et al. Vacuolar protein sorting: two different functional states of the AAA-ATPase Vps4p. J Mol Biol. 2008; 377:352–363. [PubMed: 18272179]
36. Landsberg MJ, Vajjhala PR, Rothnagel R, Munn AL, Hankamer B. Three-dimensional structure of AAA ATPase Vps4: advancing structural insights into the mechanisms of endosomal sorting and enveloped virus budding. Structure. 2009; 17:427–437. [PubMed: 19278657]
37. Yu Z, Gonciarz MD, Sundquist WI, Hill CP, Jensen GJ. Cryo-EM structure of dodecameric Vps4p and its 2:1 complex with Vta1p. J Mol Biol. 2008; 377:364–377. [PubMed: 18280501]
38. Garrus J, et al. Tsg101 and the vacuolar protein sorting pathway are essential for HIV-1 budding. Cell. 2001; 107:55–65. [PubMed: 11595185]
39. Lata S, et al. Helical structures of ESCRT-III are disassembled by VPS4. Science. 2008; 321:1354–1357. [PubMed: 18687924]
40. Glynn SE, Martin A, Nager AR, Baker TA, Sauer RT. Structures of asymmetric ClpX hexamers reveal nucleotide-dependent motions in a AAA+ protein-unfolding machine. Cell. 2009; 139:744–756. [PubMed: 19914167]
41. Stinson BM, et al. Nucleotide binding and conformational switching in the hexameric ring of a AAA+ machine. Cell. 2013; 153:628–639. [PubMed: 23622246]
42. Hersch GL, Burton RE, Bolon DN, Baker TA, Sauer RT. Asymmetric interactions of ATP with the AAA+ ClpX6 unfoldase: allosteric control of a protein machine. Cell. 2005; 121:1017–1027. [PubMed: 15989952]
43. Briggs LC, et al. Analysis of nucleotide binding to P97 reveals the properties of a tandem AAA hexameric ATPase. J Biol Chem. 2008; 283:13745–13752. [PubMed: 18332143]
44. Stinson BM, Baytshtok V, Schmitz KR, Baker TA, Sauer RT. Subunit asymmetry and roles of conformational switching in the hexameric AAA+ ring of ClpX. Nat Struct Mol Biol. 2015; 22:411–416. [PubMed: 25866879]
45. Azmi I, et al. Recycling of ESCRTs by the AAA-ATPase Vps4 is regulated by a conserved VSL region in Vta1. J Cell Biol. 2006; 172:705–717. [PubMed: 16505166]
46. Merrill SA, Hanson PI. Activation of human VPS4A by ESCRT-III proteins reveals ability of substrates to relieve enzyme autoinhibition. J Biol Chem. 2010; 285:35428–35438. [PubMed: 20805225]
47. Han H, et al. Binding of Substrates to the Central Pore of the Vps4 ATPase is Autoinhibited by the Microtubule Interacting and Trafficking (MIT) Domain and Activated by MIT Interacting Motifs (MIMs). J Biol Chem. 2015; 290:13490–13499. [PubMed: 25833946]
48. Olivares AO, Nager AR, Iosefson O, Sauer RT, Baker TA. Mechanochemical basis of protein degradation by a double-ring AAA+ machine. Nat Struct Mol Biol. 2014; 21:871–875. [PubMed: 25195048]
49. Wendler P, Ciniawsky S, Kock M, Kube S. Structure and function of the AAA+ nucleotide binding pocket. Biochim Biophys Acta. 2012; 1823:2–14. [PubMed: 21839118]
50. Yang B, Stjepanovic G, Shen Q, Martin A, Hurley JH. Vps4 disassembles an ESCRT-III filament by global unfolding and processive translocation. Nat Struct Mol Biol. 2015; 22:492–498. [PubMed: 25938660]

51. Thomsen ND, Berger JM. Running in reverse: the structural basis for translocation polarity in hexameric helicases. Cell. 2009; 139:523–534. [PubMed: 19879839]
52. Forster F, Unverdorben P, Sledz P, Baumeister W. Unveiling the long-held secrets of the 26S proteasome. Structure. 2013; 21:1551–1562. [PubMed: 24010714]
53. Zhao M, et al. Mechanistic insights into the recycling machine of the SNARE complex. Nature. 2015; 518:61–67. [PubMed: 25581794]
54. Konarev PV, Petoukhov MV, Volkov VV, Svergun DI. ATSAS 2.1, a Program Package for Small-Angle Scattering Data Analysis. Journal of Applied Crystallography. 2006; 39:277–286.
55. Putnam CD, Hammel M, Hura GL, Tainer JA. X-ray solution scattering (SAXS) combined with crystallography and computation: defining accurate macromolecular structures, conformations and assemblies in solution. Q Rev Biophys. 2007; 40:191–285. [PubMed: 18078545]
56. Konarev PV, Volkov VV, Sokolova AV, Koch MHJ, Svergun DI. PRIMUS: a Windows PC-based system for small-angle scattering data analysis. J. appl. Cryst. 2003; 36:1277–1282.
57. Svergun DI. Determination of the regularization parameter in indirect-transform methods using perceptual criteria. J. Appl. Crystallogr. 1992; 25:495–503.
58. Kabsch W. Xds. Acta Crystallogr D Biol Crystallogr. 2010; 66:125–132. [PubMed: 20124692]
59. McCoy AJ, et al. Phaser crystallographic software. J Appl Crystallogr. 2007; 40:658–674. [PubMed: 19461840]
60. Wang X, Snoeyink J. Defining and computing optimum RMSD for gapped and weighted multiple-structure alignment. IEEE/ACM Trans Comput Biol Bioinform. 2008; 5:525–533. [PubMed: 18989040]
61. Skubak P, Pannu NS. Automatic protein structure solution from weak X-ray data. Nat Commun. 2013; 4:2777. [PubMed: 24231803]
62. Emsley P, Lohkamp B, Scott WG, Cowtan K. Features and development of Coot. Acta Crystallogr D Biol Crystallogr. 2010; 66:486–501. [PubMed: 20383002]
63. Murshudov GN, Vagin AA, Dodson EJ. Refinement of Macromolecular Structures by the Maximum-Likelihood Method. Acta Crystallographica Section D. 1997; 53:240–255.
64. CCP4. The CCP4 suite: programs for protein crystallography. Acta Crystallogr. D Biol. Crystallogr. 1994; 50:157–163.
65. Adams PD, et al. PHENIX: a comprehensive Python-based system for macromolecular structure solution. Acta Crystallogr D Biol Crystallogr. 2010; 66:213–221. [PubMed: 20124702]
66. Joosten RP, Long F, Murshudov GN, Perrakis A. The PDB_REDO server for macromolecular structure model optimization. IUCrJ. 2014; 1:213–220.

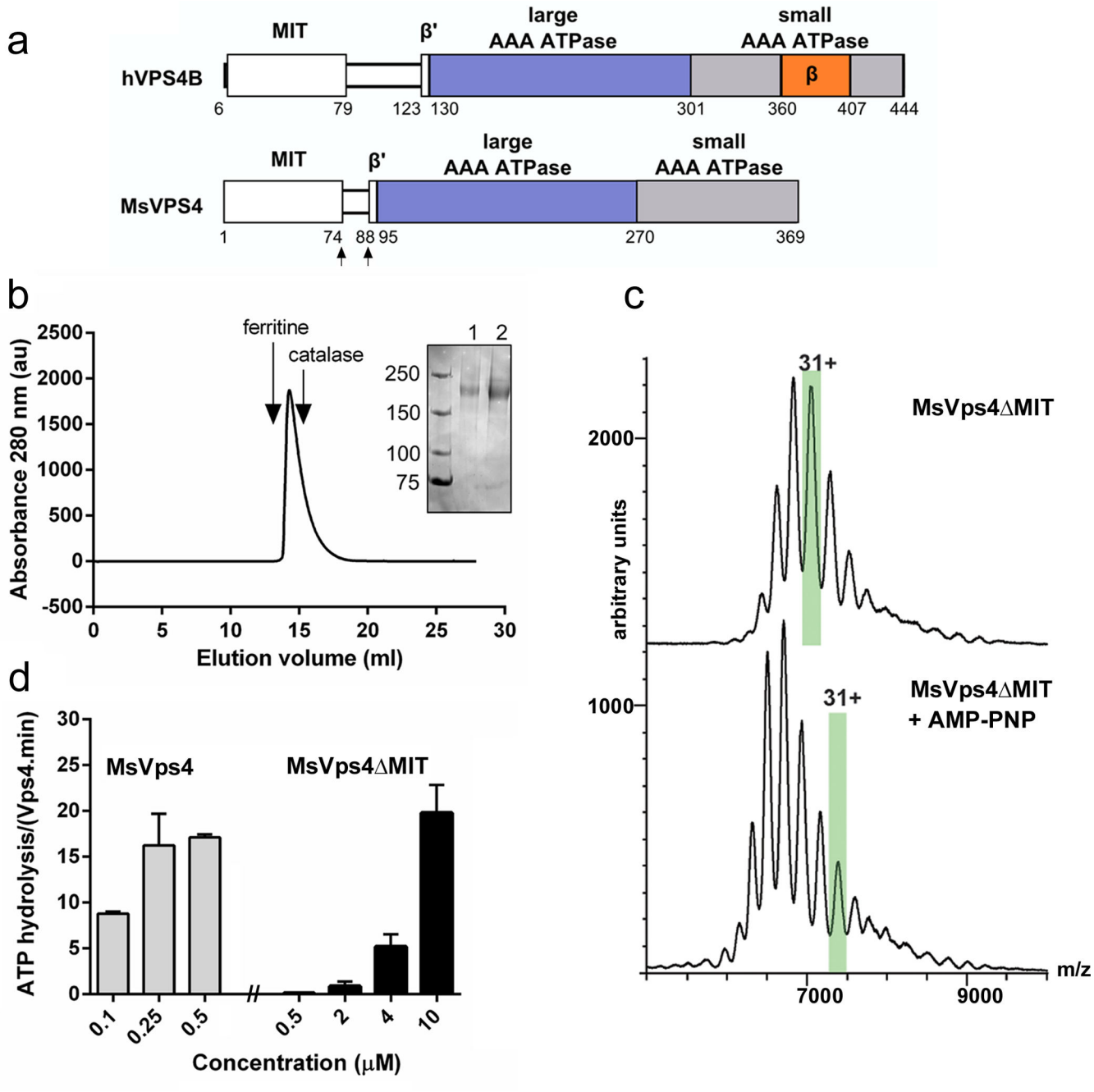

Figure 1. Biochemical and enzymatic analysis of recombinant MsVps4ΔMIT

(a) Domain organization of hVPS4B and MsVps4. MsVps4 was expressed as wild type or with N-terminal deletions (residues 75 to 369 and residues 88 to 369).

(b) Elution profile of MsVps4ΔMIT (200μM) from a Superose 6 SEC column. The elution peak of molecular sizing markers ferritin (450 kDa) and catalase (250 kDa) are indicated. Insert, SDS-PAGE analysis of MsVps4ΔMIT cross-linked with glutaraldehyde in absence (lane 1) and presence (lane 2) of 1 mM AMP-PNP and 1mM Mg acetate. Hexamer formation was confirmed by native mass spectrometry.

(c) Mass spectra of the cross-linked MsVps4ΔMIT in absence (top spectrum) and presence of AMP-PNP (bottom spectrum). MsVps4ΔMIT is hexameric in both conditions. The mass of MsVps4ΔMIT in presence of AMP-PNP is larger than in absence of the non hydrolysable ATP analogue. This greater mass is most likely due to a covalent binding of the AMP-PNP. The ions carrying 31 charges (31+), highlighted in green, illustrate the mass difference between the two samples.

(d) ATP hydrolysis of full length MsVps4 and MsVps4ΔMIT at 60°C. Values reported represent mean ± standard deviation of three independent experiments carried out on at least two different batches of purified Vps4.

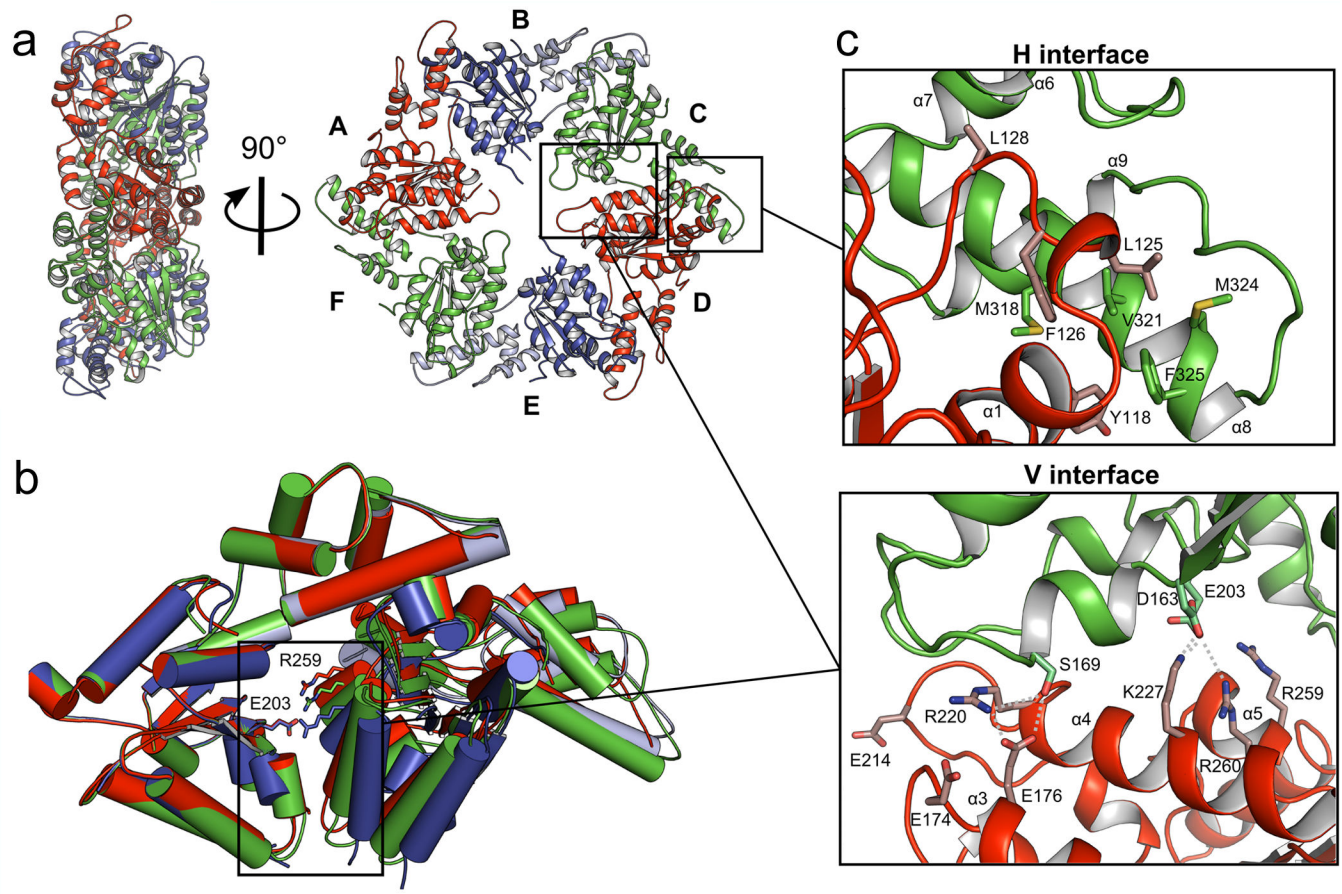

Figure 2. Crystal structure of the MsVps4ΔMIT pseudohexamer

(**a**) Cartoon representation of the MsVps4ΔMIT pseudohexamer viewed from two orientations. Asymmetric MsVps4ΔMIT has twofold non-crystallographic symmetry with opposing protomers making identical interactions. The protomers are labeled from A to F and identical protomers are represented in the same color, except for protomers B and E, whose small ATPase domain is shown in light blue and the large ATPase domain in dark blue. (**b**) Superposition of the three different dimers present in the pseudohexamer, formed by A – B, B – C and C – D. The dimeric substructures are superimposed by aligning the large ATPase domain of the first protomer. This superposition reveals different positions of the large ATPase domain of the second protomer. The catalytic Glu203 (left subunit) and the arginine finger residue Arg259 (right subunit) are represented with sticks. (**c**) Molecular interactions at the H interface of the C–D dimer and (**d**) molecular interactions at the variable V interface of the same dimer. A list of the molecular interactions of the three interfaces is shown in Supplementary Table 1.

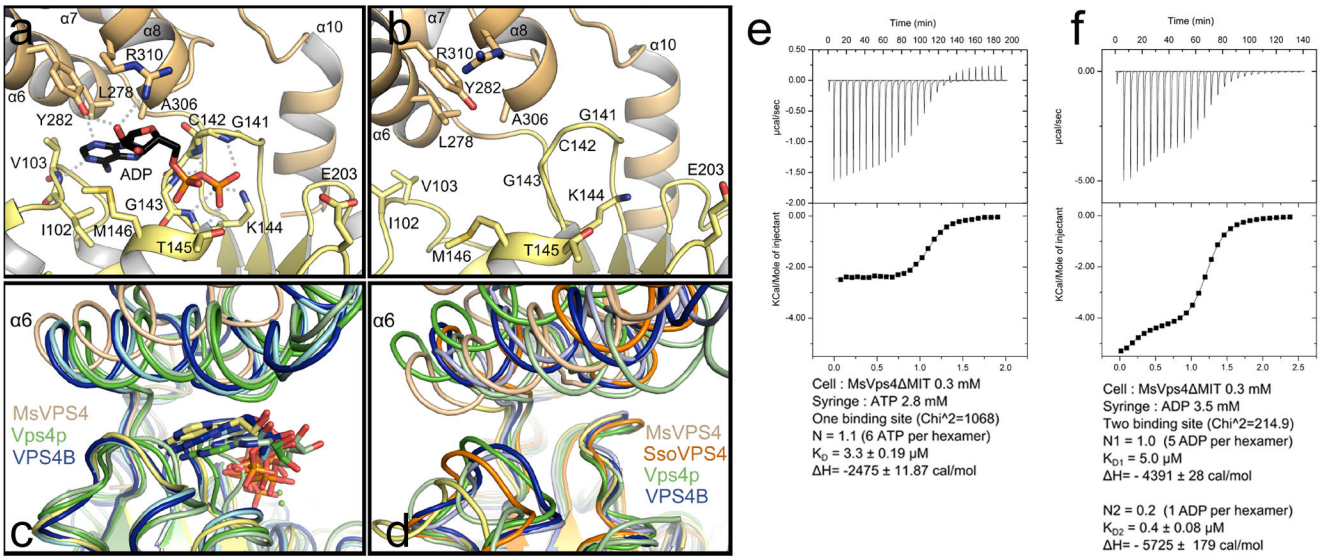

Figure 3. Crystal structure of MsVps4ΔL-MIT bound to ADP

View of the nucleotide binding site. (**a**) Structure of ADP bound MsVps4ΔL-MIT. The MsVps4ΔL-MIT large ATPase domain (yellow) and small ATPase domain (beige) are represented in cartoon. ADP and interacting residues are shown as sticks and colored by atom type. Polar interactions are indicated by grey dashes. (**b**) Close-up of the nucleotide binding site of apo MsVps4ΔMIT (protomer F). (**c**) Superposition of the ADP-bound MsVps4ΔL-MIT (yellow and beige), ATPγS-bound yeast Vps4 (green, pdb 3EIH), ADP-bound yeast Vps4 (pale green, pdb 2QPA), ATP-bound mouse VPS4B (blue, pdb 2ZAN) and ADP-bound mouse VPS4B (pale blue, pdb 2ZAO). (**d**) Superposition of different Vps4 structures with no nucleotide bound. Superposition of apo MsVps4ΔMIT (yellow and beige), apo SsoVps4 (orange, pdb 4LGM, Cl^- bound in the P-loop), yeast Vps4p (green, pdb 3EIH, molecule C, ethylene glycol-Mg^{2+} bound in the P-loop), apo yeast Vps4p (pale green, pdb 2RKO), human VPS4B (blue, pdb 1XWI, SO_4 bound in the P-loop) and mouse VPS4B (pale blue, pdb 2ZAM). The structures are superimposed by aligning the large ATPase domains. Nucleotides are represented in sticks in the same color as the corresponding structures.

(e) ITC analyses of ATP binding to MsVps4ΔMIT. ITC data were recorded upon successive injection of ATP into the cell containing 300 µM MsVps4ΔMIT, which permits nucleotide-independent hexamer formation. This revealed a 1:1 binding mode for ATP.

(f) ITC analyses of ADP binding to MsVps4ΔMIT at a concentration of 300 µM. The experimental data fits best to a two binding site model with one high affinity binding site and 5 lower affinity binding sites. Experiments shown in e and f were repeated three times.

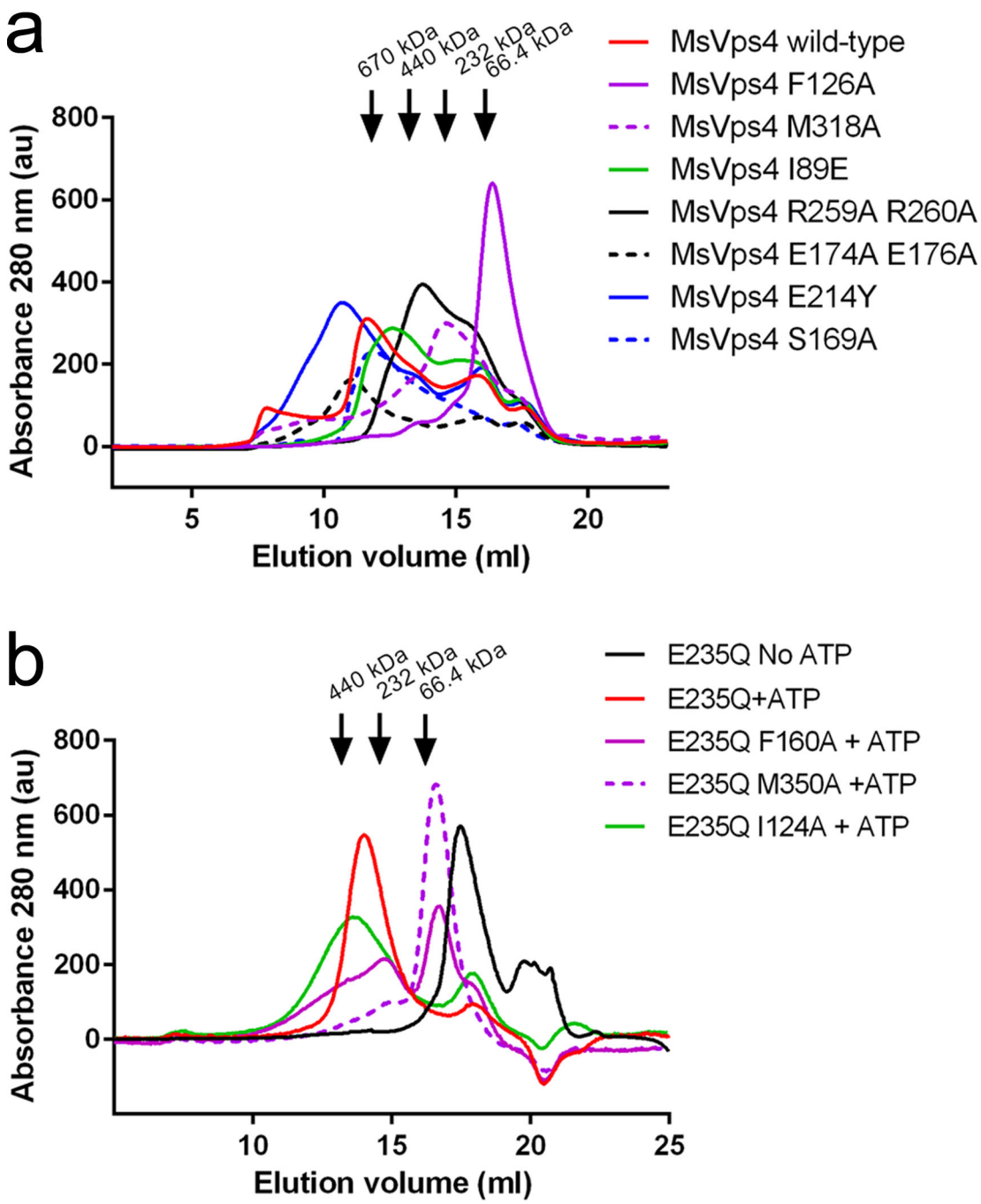

Figure 4. SEC analysis of MsVps4 and hVPS4B wild type and mutants

(a) Wild type full length MsVps4 and mutants thereof were separated on a superpose 6 size exclusion chromatography column at a protein concentration of 70 μM that induces dodecamer formation. The elution peak of molecular sizing markers thyroglobulin (660 kDa), ferritin (450 kDa), catalase (250 kDa) and bovine serum albumin (66.4 kDa) are indicated **(b)** The catalytic mutant of hVPS4B (E235Q) and mutants thereof were separated on a superose 6 column at a concentration of 100 μM and in the presence of 1 mM ATP and

5 mM $MgCl_2$, which induces hexamer formation. The elution positions of marker proteins are indicated.

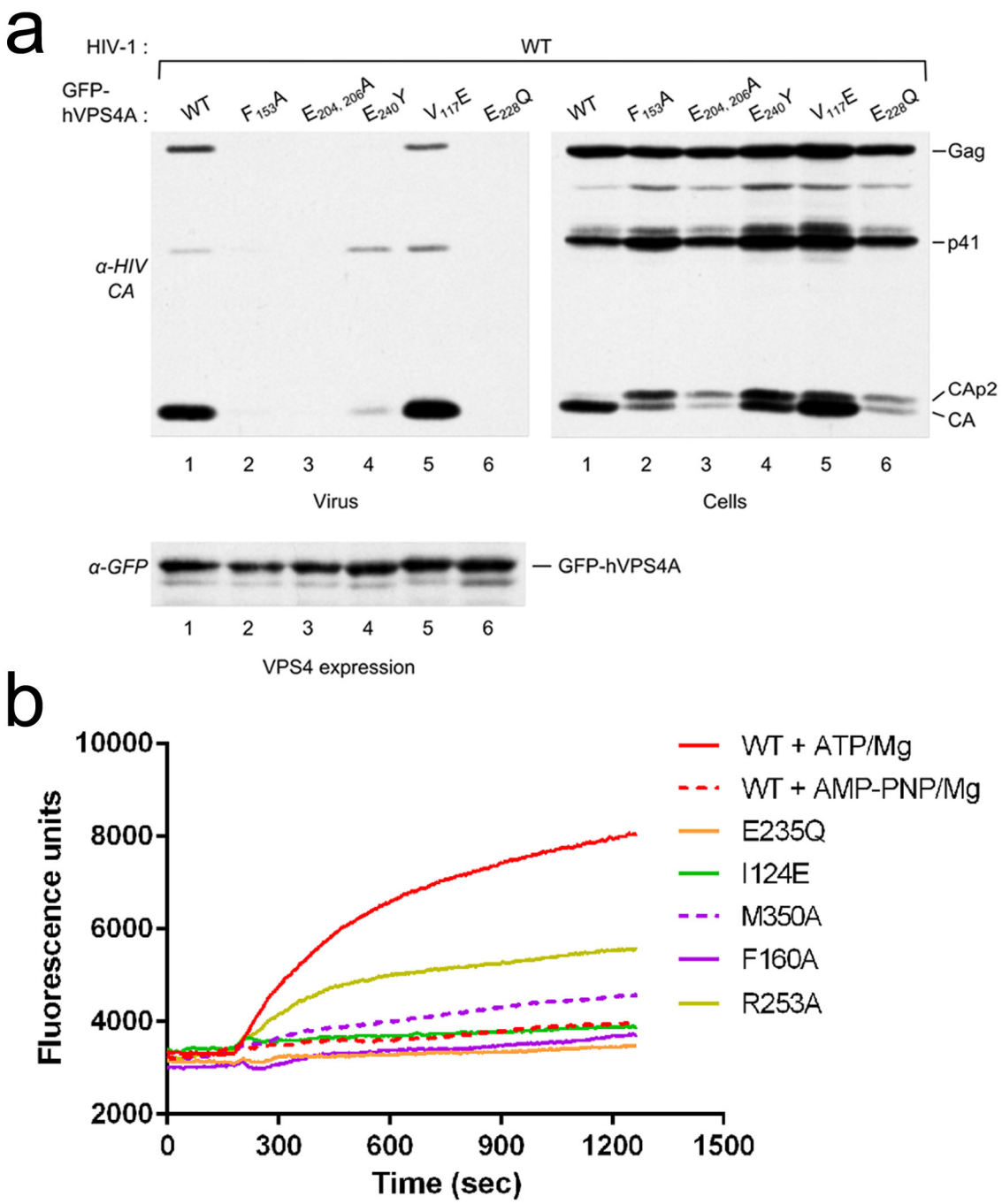

Figure 5. Mutations within hVps4 affect HIV-1 budding and ESCRT-III disassembly *in vitro*

(a) 293T cells were cotransfected with HIV-1 proviral DNA and vectors expressing GFP fused to WT hVps4A or to the indicated hVPS4A mutants. Virus release (upper left panel) and intracellular Gag processing were examined by Western blotting with an anti- HIV-1 CA antibody (upper right panel). The expression levels of WT and mutant GFP-VPS4A were compared by Western blotting with an anti-GFP antibody (lower panel).

(b) Disassembly of fluorescein-labeled ESCRT-III CHMP2AΔC-CHMP3 helical tubes measured by change in fluorescence emission intensity upon addition of VPS4B plus ATP

and Mg^{2+} (red); MsVps4 plus AMP-PNP and Mg^{2+},(red dashed line) and mutants of hVPS4B plus ATP and Mg^{2+} as indicated (I124E, green; M350A magenta dashed line; F160, magenta; R253A, yellow). The experiment was repeated three times.

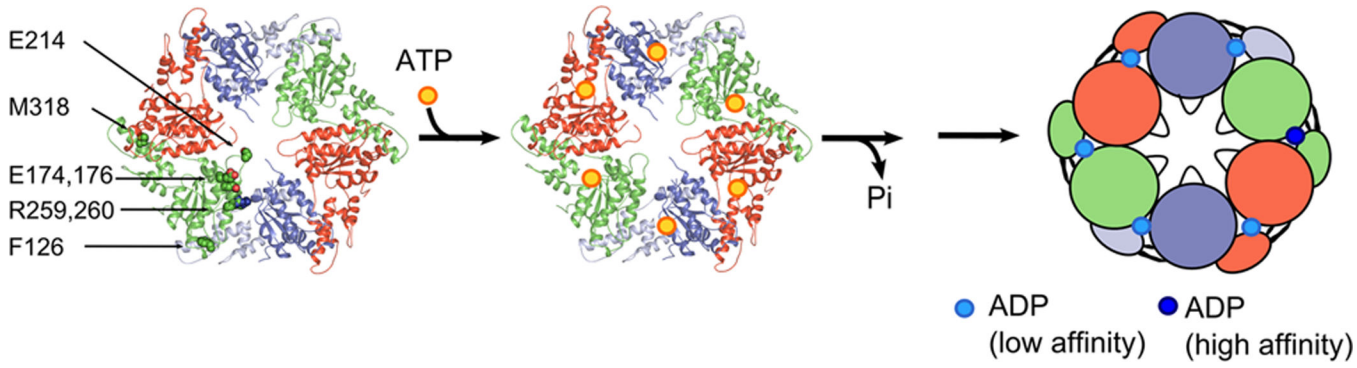

Figure 6. Model for Vps4 action

The MsVpsΔMIT pseudohexamer is represented as a cartoon, with identical protomers shown in the same color. (**a**) The nucleotide free pseudohexamer, (**b**) the pseudohexamer may bind six ATP (yellow sphere), which are likely required to assemble the catalytic active ring structure, (**c**) ATP hydrolysis generates intermediate states, which leads at one point of the cycle to an intermediate conformation that binds one ADP with high affinity and 5 with low affinity. The position of the arginine fingers, the glutamate (174, 176) V interface residues, the pore loop glutamate (214) and phenylalanine 126 are indicated. These residues are required for ATPase activity and most likely participate in the transfer of ATP hydrolysis induced conformational changes of two opposing monomers to their neighbors, thereby powering the disassembly of ESCRT-III substrate complexes via the central pore[47,52].

Table 1

Crystallographic data collection and refinement statistics.

Data collection	**MsVps4ΔMIT**	**ADP/ MsVps4ΔL-MIT**	**ADP/ MsVps4ΔMIT**
Space group	P212121	P65	P65
Cell dimensions			
a, *b*, *c* (Å)	99.70, 127.39, 191.23	65.27, 65.27, 112.5	151.19, 151.19, 98.59
α, β, γ (°)	90, 90, 90	90, 90, 120	90, 90, 120
Resolution (Å)	48–3.6 (3.8–3.6)*	2.4 (2.49–2.40)*	3.2 (3.4–3.2)*
R_{merge}	9.1 (61.6)	5.8 (63.1)	14.4 (51)
$I / \sigma I$	8.31 (1.76)	16.7 (2.3)	9.9 (3.1)
Completeness (%)	99.1 (99.6)	99.7 (99.7)	99.6 (99.8)
Redundancy	5.3 (5.5)	4.1 (4.2)	4.6 (4.7)
Refinement			
Resolution (Å)	3.6	2.4	3.2
No. reflections	27368	10642	21217
R_{work} / R_{free}	26.4/31.8	21.2/26.4	22.9/26.8
No. atoms			
Protein	12875	2133	6528
Ligand/ion	0	27	81
Water	0	7	12
B-factors			
Protein	142.61	55.8	53.5
Ligand/ion		43.1	43.1
Water		41.7	21.2
R.m.s deviations			
Bond lengths (Å)	0.01	0.013	0.011
Bond angles (°)	1.716	1.59	1.54

*1 crystal was used for each structure.*Highest resolution shell is shown in parenthesis.

Table 2

Summary of oligomeric states, enzymatic activity, ESCRT-III disassembly and HIV-1 budding of MsVps4 and hVPS4A and B constructs.

MsVps4 and hVPS4 constructs	Domain	Elution volumes (ml)				Complex[1]	ATPase[2]	ESCRT-III[3]	HIV-1[4]
MsVps4_wild-type		11.6	13.4	15.8	17.1	dodecamer	100%	-	-
hVPS4B_E235Q +ATP			14.1		17.8	hexamer	-	-	-
hVPS4B_wild-type +ATP/Mg		-	-	-	-	-	100%	100%	
hVPS4A_wild type		-	-	-	-	-	-	-	100%
MsVps4_Phe126Ala	H				16.4	monomer	0.0 ± 0.1%	-	-
hVPS4B_E235Q_Phe160Ala + ATP			14.7	16.7	17.9	monomer	-	-	-
hVPS4B_Phe160Ala + ATP/Mg		-	-	-	-	-	0.0 ± 0.1%	Inhib.	-
hVPS4A_Phe153Ala		-	-	-	-	-	-	-	Inhib.
MsVps4_Met318Ala	H		13.1	14.6	17.2	hexamer	154 ± 2,5%	-	-
hVPS4B_E235Q_Met350Ala + ATP				14.3	16.6	monomer		-	-
hVPS4B_Met350Ala + ATP/Mg		-	-	-	-	-	0.0 ± 0.1%	~20%	-
MsVps4_Ile89Glu	AAA		12.6	15.8	17.5	dodecamer	85.6 ± 16.4%	-	-
hVPS4B_E235Q_Ile124Glu + ATP			13.6		18	hexamer	-	-	-
hVPS4B_Ile124Glu + ATP/Mg		-	-	-	-	-	8.10 ± 1.95%	Inhib.	-
hVPS4A_Val117Glu		-	-	-	-	-	-	-	100%
MsVps4_Glu174Ala_Glu176Ala	V	10.5	13.7	16	17.6	dodecamer	0.14 ± 0.1%	-	-
hVPS4A_Glu204Ala_Glu206Ala		-	-	-	-	-	-	-	Inhib.
MsVps4_Arg259Ala_Arg260Ala	V		13.7	15.4	17.3	hexamer	0.1 ± 0.02%		-
MsVps4_Glu214Tyr	pore loop 2	10.7	13.5	15.9	17.6	dodecamer	7.9 ± 1.5%	-	-
hVPS4A_Glu240Tyr		-	-	-	-	-	-	-	Inhib.
MsVps4_Ser159Ala	V	11.9	14.6	-	17.4	dodecamer	14.5 ± 3.2%	-	-
hVPS4B_Arg253Ala + ATP/Mg	V	-	-	-	-	-	69.5 ± 5%	~50%	-

[1] Main complex formed *in vitro*

[2] ATPase activity ; reported ATPase values correspond to the mean ± SD of at least 3 distinct experiments carried out on 2 or more batches of MsVps4.

[3] Disassembly of ESCRT-III CHMP2A-CHMP3 tubular structures

[4] Inhibition (Inhib.) of HIV-1 budding